Check for updates

Production of boron nitride/titanium dioxide composite nanofibers *via* sustainable electrospinning methods and their environmentally friendly photocatalytic and antibacterial applications†

Ramazan Bayat,[ab] Ebru Halvaci,[a] Muhammed Bekmezci,[ab] Güray Kaya,[b] Hüseyin Bogac Poyraz,[c] Idris Kaynak[d] and Fatih Sen [ID] *[ae]

Low-cost and environmentally friendly nanomaterials fabricated using sol–gel, electrospinning, hydrothermal and solvothermal methods are highly important for the removal of dyes (which are important water pollutants) from water sources and for reducing biological activity on the membrane surface of treatment facilities. In this study, boron nitride/titanium dioxide composite nanofibers (BTFs) were synthesized using an electrospinning method. The structural and optical properties of the BTFs were investigated using various analytical techniques, including X-ray diffraction (XRD), scanning electron microscopy (SEM), ultraviolet-visible spectroscopy (UV-vis) and Fourier transform infrared spectroscopy (FTIR), and then, their capability for photocatalytic dye removal and antibacterial activity was studied. SEM analysis of the characterized BTF nanofibers showed that the fiber structures were random, distant from each other and formed networks. Furthermore, the band energy calculated from the UV-vis spectrum was 2.81 eV. Subsequently, the catalytic activity for the removal of methylene blue and rhodamine B dyes from water was determined to be 83.7% and 84.3%, respectively. In addition, the BTF nanofibers exhibited a high antibacterial effect against *Escherichia coli*, *Staphylococcus aureus*, *Bacillus subtilis* and *Klebsiella pneumoniae* bacteria. In addition, antibacterial tests revealed that the bacterial culture containing BTF nanofibers showed a lethal effect even at low concentrations. Thus, BTF nanofibers are envisaged to play important roles in water purification and microorganism-control applications owing to their advantages of environmental friendliness, low-cost, and sustainability.

1. Introduction

Environmental pollution continues to be a major threat to humanity with the rapid development of industries, and it is one of the leading causes of various diseases and deaths. However, the most contributing factors for urbanization, industrialization and their accompanying environmental pollution worldwide are human activities. To build a secure future, clean water resources and the universal supply of fresh water are critical requirements for humanity.[1–3] In this context, industrial wastes, particularly from the textile, cosmetic and plastic industries and dyestuffs and organic dyes, have been identified as the primary sources of pollutants in water resources. High microbial activity and turbid coloration observed in water contaminated with industrial waste present significant challenges for both the nature and humanity. Even at low concentrations, the contamination of drinking water with dyes can result in serious health issues.[4–7] In the water treatment industry, chemical disinfectants and membrane treatment technologies are potential solutions for freshwater production.[8] However, the chemical disinfectants used are known to have carcinogenic effects over time, and membrane technology systems are very difficult systems to control during water treatment and are prone to biofilm formation on the membrane surface, increasing biofouling. Therefore, new approaches are needed to remove organic pollutants from water and reduce biological activity on the membrane surface in treatment facilities.[9] The momentum gained by microbiology and nanotechnology in recent years offers new developments in this field.

aSen Research Group, Department of Biochemistry, Dumlupinar University, Kutahya, Türkiye. E-mail: fatihsen1980@gmail.com

bDepartment of Materials Science & Engineering, Faculty of Engineering, Dumlupinar University, Kutahya, Türkiye

cEskisehir Technical University, Iki Eylul Campus, Faculty of Engineering, Department of Materials Science and Engineering, Eskisehir, 26555, Türkiye

dMachinery and Metal Technologies, Vocational School of Technical Sciences, Usak University, 1 Eylul Campus, 64200 Usak, Türkiye

eSRG Incorporated Company, Kutahya Design & Technopole, Calca OSB Neighbourhood, 43100 Kutahya, Türkiye

† Electronic supplementary information (ESI) available. See DOI: https://doi.org/10.1039/d4ra09118c

Recent advances in nanotechnology are known to provide desirable functional properties, such as the efficient design, characteristics and specification of nanoparticles.[10–19] Nanoparticles are obtained using special techniques owing to their shape-controlled, highly porous, and flexible composite structures. These structures are obtained by combining many techniques, especially sol–gel, electrospinning, hydrothermal and solvothermal methods.[20,21] These methods show promise in developing low-cost and environmentally friendly methods for the production of fresh water using nanoparticles. Owing to the photocatalysis properties of nanoparticles obtained *via* various methods, they can play important roles in the conversion of solar energy and remediation of organic pollutants.[22] Photocatalysis reactions are very useful methods for removing organic dyes and bacterial contaminants from water treatment systems. In this regard, among the semiconductor materials, metal compounds such as tin(IV) oxide (SnO_2), nickel oxide (NiO), zinc oxide (ZnO), and titanium dioxide (TiO_2), are the most efficient and environmentally friendly nanoparticle structures that show photocatalysis properties.[23] In particular, TiO_2 nanoparticles are cost-effective photocatalysts for the degradation of organic dyes owing to their composite structure, non-toxic nature, and excellent optical, chemical and physical properties.[24] TiO_2 is the most widely used semiconductor catalyst for photocatalysis studies owing to its unique properties such as high chemical stability, low toxicity and fast oxidation reaction.[25] However, owing to the inefficient utilization of photogenerated electron–hole pairs, the activity of semiconducting TiO_2 compounds needs to be enhanced. Suppression of the photogenerated electron–hole pair combinations in semiconductor assembly is known to increase the net charge transfer in solar cells and photocatalysis reactions.[26] To achieve this, two semiconductor nanoparticles should be paired using acyl group materials. Accordingly, TiO_2–SnO_2 has been the subject of various researches as it consists of two semiconductor oxides.[27,28] When two semiconductor particles are attached to the SnO_2 band, they degenerate the photogenerated electrons. Meanwhile, the TiO_2 particles are concentrated on the valence band as the electron–hole pairs start to flow *via* their interaction with the light. Sn metal increases the charging rate of TiO_2 as a result of a light-induction effect.[29–31] In addition, boron nitride (BN) is often used as a support material in optoelectronic and nanoelectronic device applications owing to its different chemical and physical properties.[32] Indeed, the photocatalytic activity of the BN-TiO_2 nanocomposite structure is a major research topic.[33,34] This is mainly owing to the electrostatic interaction of the positively charged TiO_2 metal accelerating the flow of the negatively charged BN nanomaterial in the composite state, thereby improving the photocatalytic activity. In this study, boron nitride/titanium dioxide composite nanofibers (BTFs) obtained *via* the electrospinning method were used for photocatalytic dye removal and antibacterial applications.

2. Experimental section

2.1. Materials

Commercial boron nitride (Aldrich, 95%) (BN), titanium tetraisopropoxide (Merck, 98%) (TIPOD), polyvinylpyrrolidone (PVP) (Sigma Aldrich, Mw = 1 300 000), methylene blue (Sigma, 97%) (MB), rhodamine B (Sigma, 95%) (RhB) and absolute ethanol (Isolab, 99.9%) were purchased and used without further purification.

2.2. BTF nanofibers production

BTF nanofibers were obtained using the electrospinning method. First, 1.6 g PVP, 0.239 g TiO_2, 0.150 g BN and 5 mL TIPOD were added to 15 mL ethanol for synthesizing the BTF nanofibers. The solution was stirred overnight at room temperature. The homogeneous solution obtained was taken into a syringe and the fibers were collected on an aluminum foil layer using 25 kV DC voltage at a flow rate of 1 mL h^{-1} in an electrospinning device. The fibers collected on the aluminum foil were calcined at 500 °C for 1 h at a temperature ramp rate of 5 °C.[35,36]

2.3. Physical and chemical characterizations

The morphological, structural and elemental analyses of the BTF nanofiber structure were characterized using SEM. To elucidate the crystal structure of the samples, a Rigaku MiniFlex model XRD device was used. Spectral analysis of the synthesized material was performed using a Perkin Elmer-Lambda 750 model UV-vis spectrometer. In addition, FTIR characterization was performed with a Perkin Elmer-Spectrum II device.

2.4. Photocatalytic activity measurements

Methylene blue (MB) and rhodamine B (RhB) dyes were considered as reference organic pollutants to evaluate the photocatalytic activity of the BTF nanofibers. The photocatalytic performance of the obtained nanomaterials was evaluated based on the decrease in the concentration of MB and RhB dye during exposure to visible-light irradiation (400 W halogen lamp). First, the solution mixture was sonicated for 30 min without irradiation to reach adsorption–desorption equilibrium for MB and RhB. The solution was then irradiated with visible light for 180 min. At intervals of 5, 10, 15 and 30 min, 3 mL of sample solution was removed from the resulting solution and centrifuged to separate the catalyst. The centrifuged solution was analyzed with a UV-vis spectrometer. The absorbance spectra of MB were recorded to measure the main absorption band around $\lambda = 660$ nm and the change in its concentration. On the other hand, the absorbance spectra of RhB were obtained and compared with the changes in the main absorption band and concentration at $\lambda \sim 550$ nm. After irradiation, the photocatalytic degradation efficiency was calculated according to the following degradation efficiency equation:

$$\text{Degradation efficiency (\%)} = [(C_0 \times C)/C_0] \times 100$$

2.5. Determination of the antibacterial activity by a microdilution method

Antibacterial activity studies of the obtained BTF nanofibers were tested against human pathogenic bacteria. Four bacterial

species, two Gram positive and two Gram negative, were selected. These were taken from *Escherichia coli (E. coli)*, *Staphylococcus aureus (S. aureus)*, *Bacillus subtilis (B. subtilis)* and *Klebsiella pneumoniae (K. pneumoniae)* stock bacterial cultures transferred to nutrient broth and placed in an oven for 24 h incubation.[37] At the end of 24 h, absorbance values were measured separately for the bacterial species and the concentrations of BTF nanofibers for the antibacterial test trials were determined according to the reference method, and were determined as 500, 250, 100, and 50 μg mL^{-1}. Antibacterial assays were prepared on a 96-well plate as 3 replicate controls. To observe the growth of bacterial culture containing BTF nanofibers and the effects of the nanoparticles, they were incubated for 24 h in a 37 °C incubator on a shaker setup. After 24 h, the absorbance values of the culture containing the BTF nanofibers were determined at 600 nm using a spectrophotometer. Cell viability and bacterial inhibition were evaluated according to the absorbance values of the bacterial cultures at different concentrations.[38,39]

3. Results and discussion

3.1. Characterizations of the BTF nanofibers

XRD of the BTF nanofibers obtained *via* electrospinning was used to analyze the crystal structure of the fibers. The sharp peaks at 2θ values of 25.81°, 38.29°, 48.4°, 54.45°, 55.29°, 63.16°, 69.18°, 70.62°, 75.33° and 83.07° in Fig. 1a were related to the (101), (004), (200), (105), (211), (204), (116), (220), (215) and (224) planes of the pure TiO_2 anatase form, respectively. Also, the weak peak at $2\theta = 27.97°$ was due to hexagonal boron nitride. Crystal structure analysis showed that BTF nanofibers had been successfully obtained in accordance with the literature.[40–42] In addition, the structural compositions of the BTF nanofibers obtained by the electrospinning method before and after calcination were also characterized by FTIR analysis, as shown in Fig. 1b. The FTIR
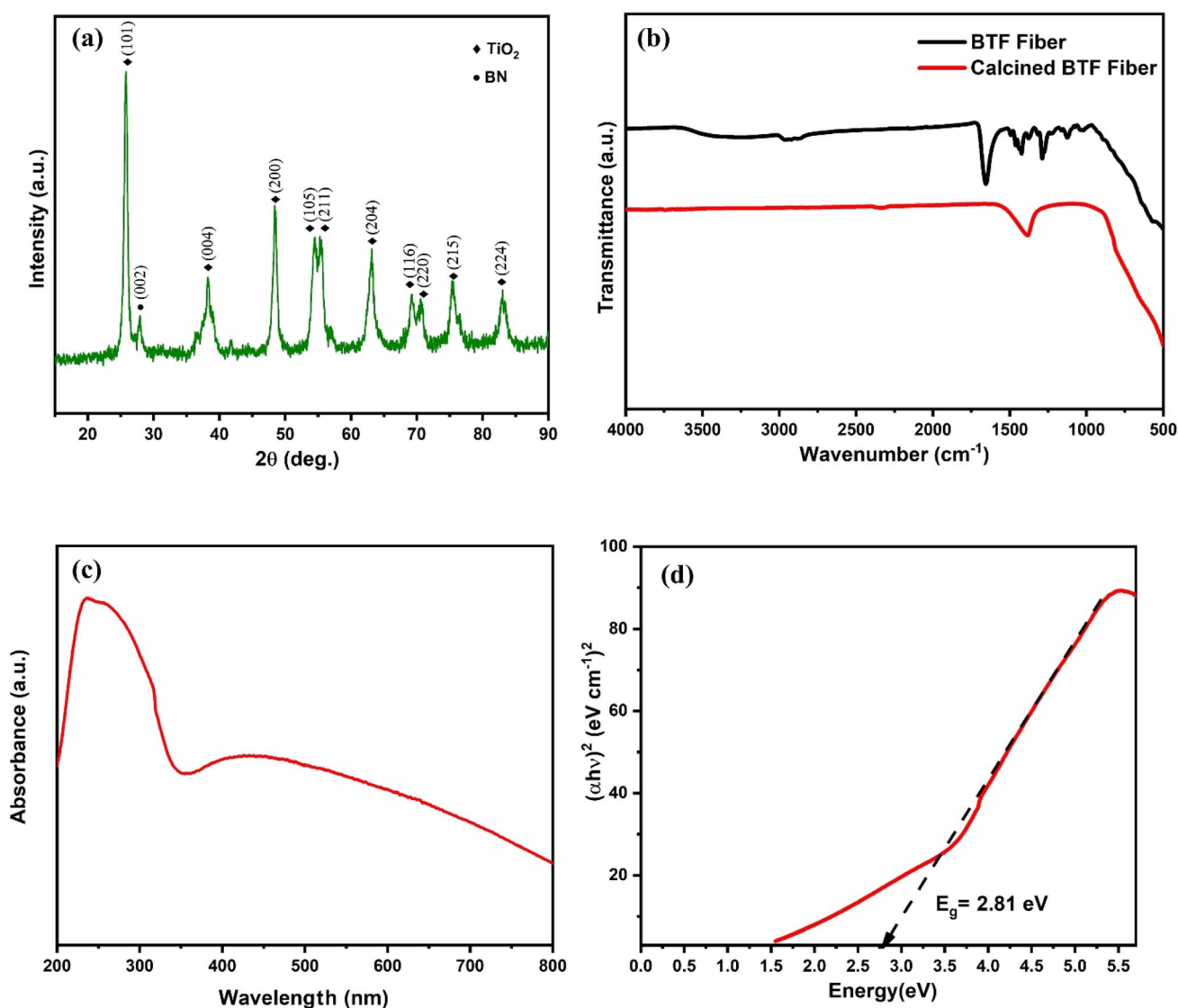

Fig. 1 XRD diffraction pattern (a), FTIR spectrum (b), UV-vis spectrum (c), and Tauc plot (d) of the BTF nanofibers annealed at 500 °C in air for 1 h.

results of the non-calcined BTF nanofibers displayed peaks at 3393 cm^{-1} for O–H, 2928 cm^{-1} for C–H, 1649 cm^{-1} for C=O, 1426 cm^{-1} for C=C bonds, and at 1282 cm^{-1} due to C–N vibrations.[43] After calcination, there was a peak at 1375 cm^{-1} showing the counter phase within the BN layers and corresponding to the B–N E_{2g} vibration mode.[44] At the same time, due to the formation of TiO_2 nanoparticles, peaks for Ti–O stretching and Ti–O–Ti bridging stretching modes were observed at 500–900 cm^{-1}.[45,46] The disappearance of the peaks belonging to PVP after calcination confirmed that the calcination process was successful.[35] The UV-vis absorption spectrum of the synthesized BTF nanofibers is shown in Fig. 1c, showing that the BTFs absorbed light at approximately 240 and 440 nm. In addition, the band gap energy of the BTF nanofibers was calculated from the UV-vis spectrum using eqn (1) with the Tauc relation.[47,48]
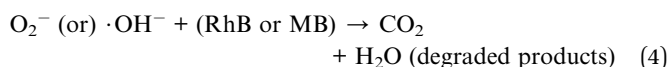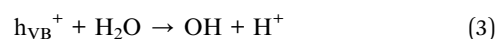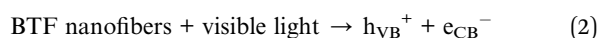
$$(\alpha h\nu)^{1/n} = A(h\nu - E_g) \tag{1}$$

As can be seen in Fig. 1d, the calculated band energy (E_g) of BTF nanofibers was 2.81 eV. This E_g value was lower than the E_g value of the pure TiO_2 nanofibers (3.20 eV). This suggests that the addition of boron nitride contributed to photocatalytic dye removal by reorganizing the energy levels of TiO_2.[33,49]

Next, SEM was used to investigate the surface morphology of the BTF nanofibers. Fig. 2 shows the SEM images of the BTF nanofibers calcined in air at 500 °C for 1 h, showing the nanofibrous morphology was maintained even after the heat-treatment process.[42] As can also be seen in the SEM images (Fig. 2a–d), the fiber structures were formed randomly, far from each other, in the form of a network, and also the fiber

structures were preserved after heat treatment. Also, it could be seen that BTF nanofibers with similar diameters were formed after calcination. Comparison of the images with the literature showed that BTF nanofibers had been successfully formed after calcination.[43,50,51]

3.2. Photocatalytic activity experiments with the BTF nanofibers

After successful synthesis and extensive characterization, photocatalytic dye removal studies of MB and RhB dyes were carried out using the BTF nanofibers. The adsorption–desorption relationship between 40 mL of MB (5 mg L^{-1}) and 40 mL of RhB (5 mg L^{-1}) solutions containing 40 mg BTF nanofibers as the initial solution was investigated. First, both solutions were stirred in the dark for 30 min in order to disperse the BTF nanofibers completely. Then, the dye removal studies in the presence of BTF nanofiber were carried out under light illumination using a metal halide lamp (400 W) at a distance of 15 cm for 180 min. The reactions of the BTF nanofibers for the photodegradation of MB and RhB dyes are briefly described below (eqn (2)–(4)).

$$\text{BTF nanofibers} + \text{visible light} \rightarrow h_{VB}^+ + e_{CB}^- \tag{2}$$

$$h_{VB}^+ + H_2O \rightarrow OH + H^+ \tag{3}$$

$$O_2^- \text{ (or) } \cdot OH^- + (\text{RhB or MB}) \rightarrow CO_2 + H_2O \text{ (degraded products)} \tag{4}$$

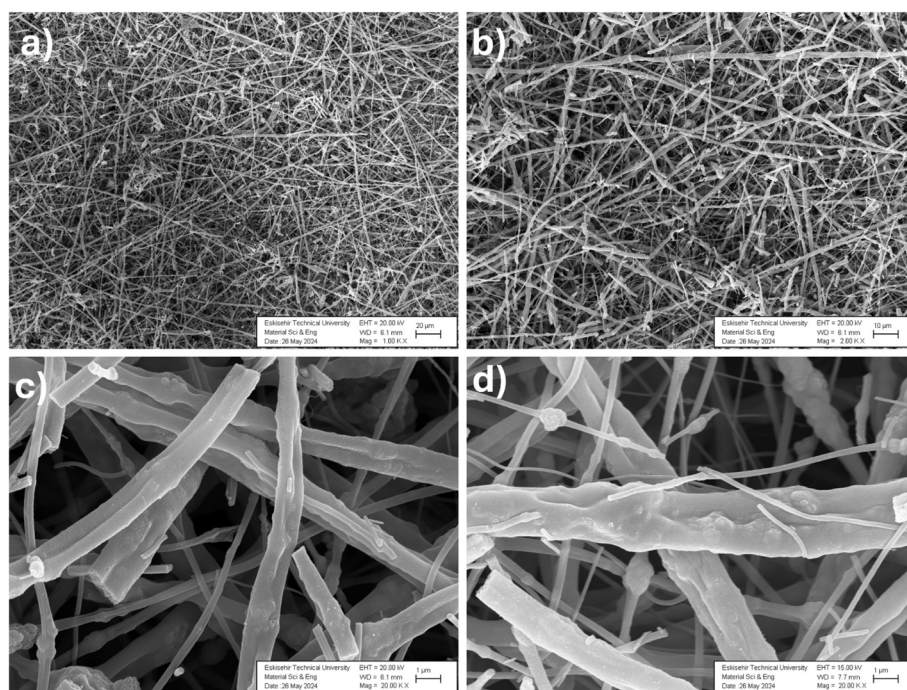The direct transition of electrons from the valence band to the conduction band on the surface of the catalysts after the

Fig. 2 SEM images of the BTF nanofibers annealed at 500 °C in air for 1 h at different magnifications of 1.0 KX (a), 2.0 KX (b), 20.0 KX and (c and d), in different regions.

absorption of light rays can lead to the production of electron (e⁻)/hole pairs (h⁺). Electrons pass from the valence band (VB) of the BTF nanofibers to the conduction band (CB) and leave gaps in the valence band in the BTF nanofibers. Electrons form

$\cdot O_2^-$ and $\cdot OH^-$ free radicals. The free radicals then react with organic dyes and cause their photodegradation.[52,53]

Fig. 3a and b show the absorbance spectra of MB and RhB. The time-dependent decrease of the characteristic peaks of both dyes indicated that the chromophore responsible for the characteristic color of the dyes was degraded in the presence of the BTF nanofiber. As shown in Fig. 3b, a shift in wavelength occurred as RhB degraded. In the photocatalytic degradation of RhB, there are two pathways, namely cleavage of the conjugated chromophore structure and N-deethylation. In the first pathway, it could be seen that the peak intensity decreased in the UV-vis spectrum, while in the second pathway, the adsorption peaks shifted toward blue wavelength.[54,55] The time-dependent % degradation plots of MB and RhB dyes are given in Fig. 3c. The decrease in the absorbance intensity of MB and RhB dyes as a function of the light exposure time shows the decrease in dye concentrations.[56] It was determined that MB and RhB dyes caused degradation of the dyes at rates of 83.68% and 84.31%, respectively, as a result of 180 min light illumination.

Following the adsorption studies, the degradation kinetics of MB and RhB dyes were calculated using first-order kinetics (eqn (5)), as shown in Fig. 4. Fig. 4a presents the photodegradation curves for the MB and RhB dyes, while Fig. 4b and c show the first-order kinetics experimental linear-fitting graphs for MB and RhB, respectively. Using the following eqn (5) for Fig. 4b, R^2 for MB was determined to be 0.921 and for Fig. 4c, R^2 for RhB was determined to be 0.897. The constant values (K) for MB and RHB were calculated as −0.00881 and −0.00882 min⁻¹, respectively, indicating the good agreement between the model and the experimental data.

$$\ln(C/C_0) = -Kt \qquad (5)$$

BTF nanofibers obtained by the electrospinning method exhibited effective catalytic performance in photodegradation processes thanks to their beneficial properties, including large surface area and high porosity. Boron doping modified the electronic structure of the titanium oxide structure, increased the light absorption and improved the photocatalytic efficiency by reducing the recombination of charge carriers. Thus, BTF nanofibers offer an important advantage in environmental applications by enabling the fast and efficient photodegradation of organic pollutants. In conclusion, the results in Table 1 show that the performance of the BTF nanofibers produced by the electrospinning method is comparable with other materials reported in the literature, and even superior to many.

3.3. Antibacterial activity experiments of the BTF nanofibers

The microdilution method was selected to determine the antibacterial activity of BTF nanofibers. Different concentrations of BTF nanofibers solution were prepared to perform *in vitro* antibacterial tests. For the antibacterial activity evaluations of the BTF nanofibers, the BTF nanofibers were tested by adding BTF nanofibers at concentrations ranging from 500 μg mL⁻¹
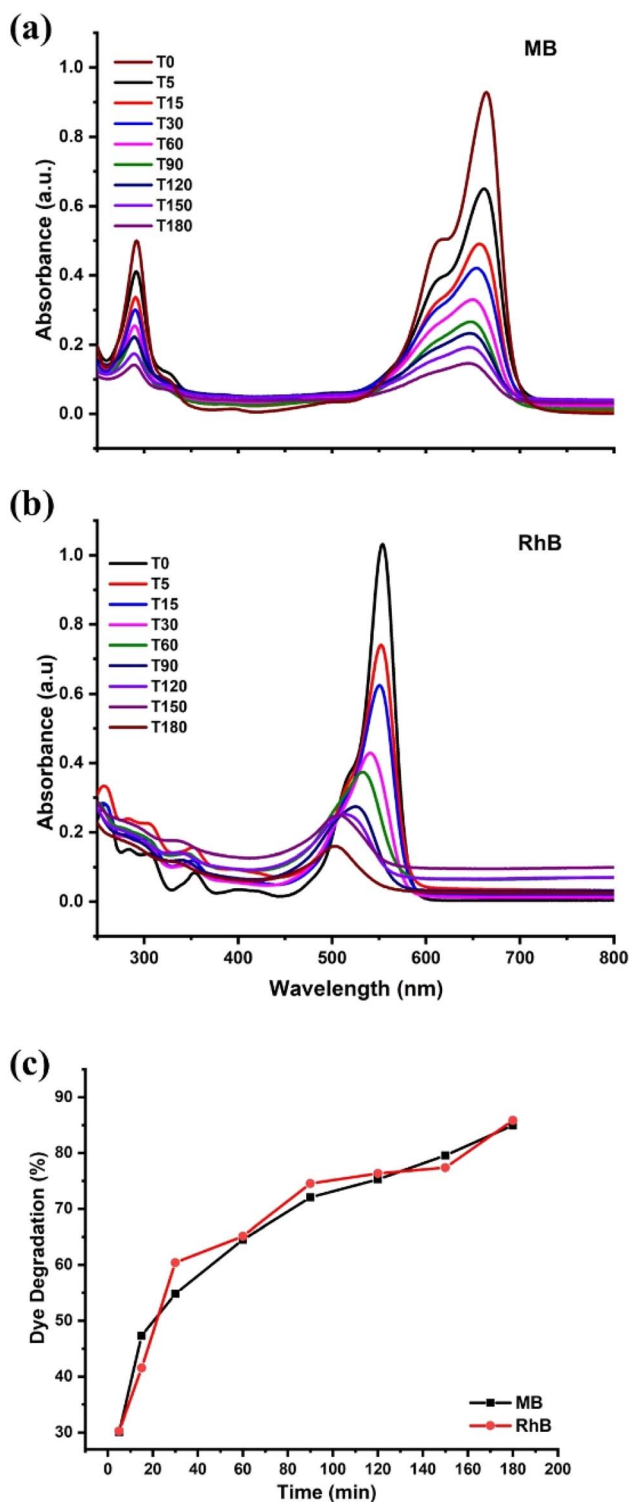

Fig. 3 UV-vis spectra for the photocatalytic degradation of MB (a), UV-vis spectra for the photocatalytic degradation of RhB (b), and percentage degradation curves for MB and RhB (c).
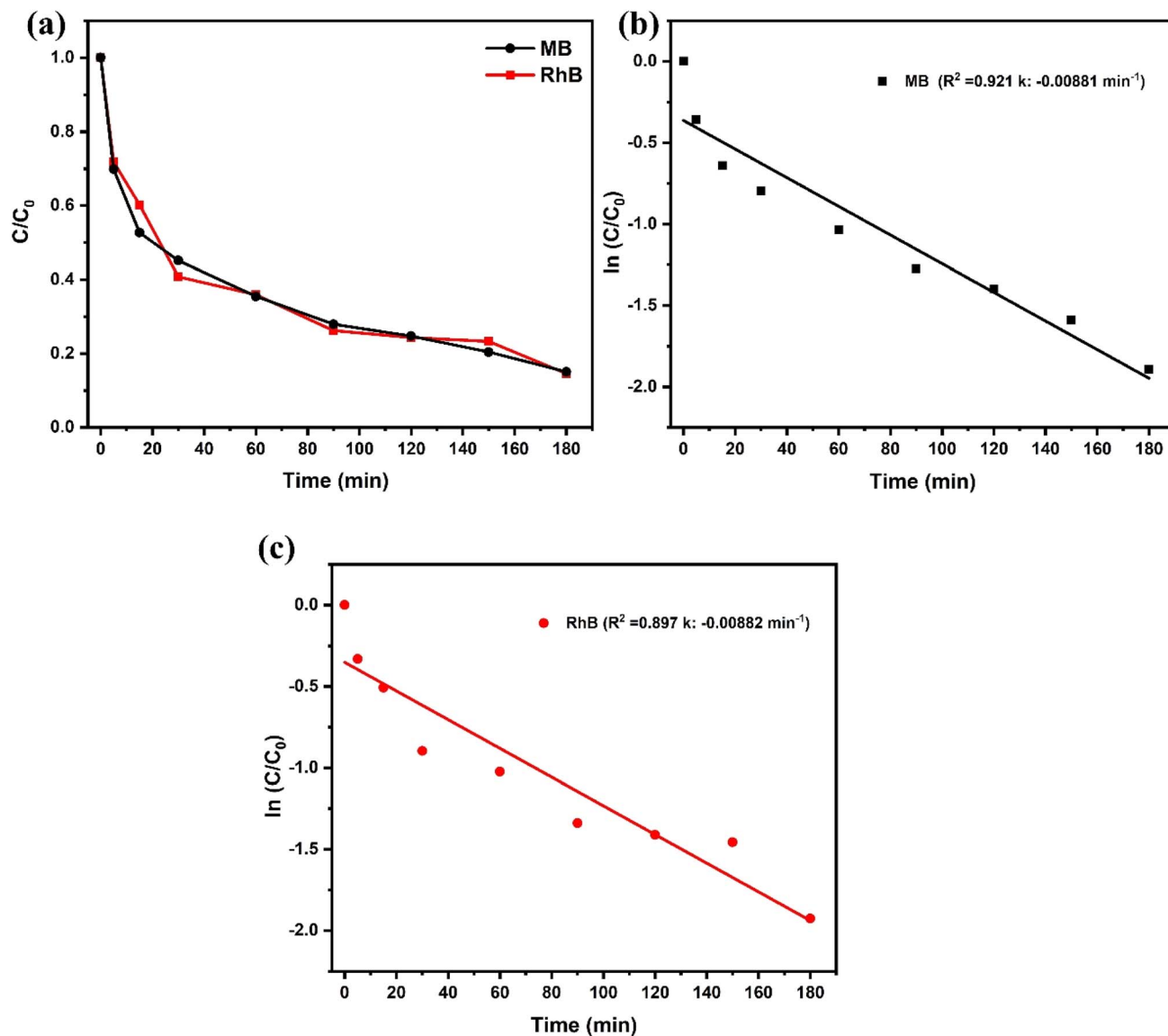
Fig. 4 Photodegradation curves of MB and RhB dyes under simulated sunlight (a) and pseudo-first-order kinetic plots for MB (b) and RhB (c).

down to 50 μg mL^{-1}. Bacterial cultures grown at 37 °C for 24 h were determined according to 0.5 McFarland standard and added to plates containing different the concentrations of BTF nanofibers.[39] The bacterial cultures containing the BTF nanofibers were incubated at 37 °C for 24 h and quantified after 24 h using a multi-plate reader (Berthold TriStar2 LB 942). The absorbance values obtained were calculated as percentage units. According to these results, it was observed that the BTF nanofibers had a killing effect against both Gram-positive and Gram-negative bacteria. As can be seen in Fig. 5, the results of this study showed that at 500 μg mL^{-1}, the BTF nanofibers had a very high antibacterial effect against *E. coli*, *S. aureus*, *B. subtilis* and *K. pneumoniae* bacteria; while the bacterial culture containing 250 μg mL^{-1} BTF nanofibers was found to have 60.68%, 57.51%, 60.31% and 59.86% killing effects, respectively. Similarly, the bacterial culture containing 100 μg mL^{-1} BTFs showed 35.35%, 42.41%, 34.78% and 27.96% killing

effects, respectively. Finally, even at the lowest concentration of 50 μg mL^{-1}, the lethal effect was 28.99%, 39.96%, 27.95%, and 16.94%, respectively.

In addition, the antibacterial activities of BTF nanofibers against *E. coli*, *S. aureus*, *B. subtilis* and *K. pneumoniae* bacteria are presented in detail in Table S1,† together with the relative standard deviation (RSD) values depending on the concentration.

In previous literature, boron nanosheets made by P. Aruna *et al.* exhibited selective toxicity against *B. subtilis*, showing a more sensitive effect on Gram-positive bacteria; however, Gram-negative bacteria (*E. coli* and *K. pneumonia*) showed resistance due to the lipopolysaccharide outer membrane, while no inhibition effect was observed against multidrug-resistant clinical isolates of *S. aureus*.[63–65] When similar studies were examined, it could be noted that the BTF nanofibers differed from other studies by showing a broad spectrum and potent

Table 1 Comparison of BTF nanofibers with other materials in the literature for dye photodegradation

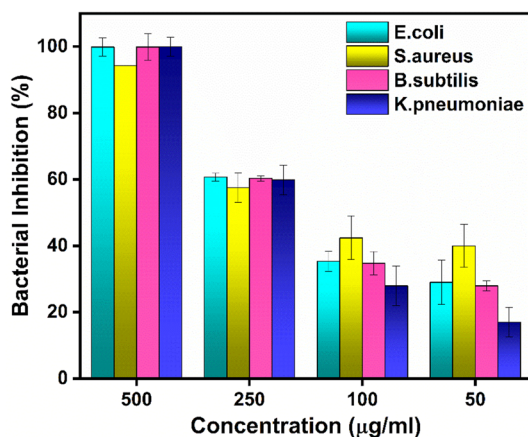| Photocatalyst	Type of dye	Photodegradation efficiency (%)	Degradation time (min)	References
Pure TiO$_2$	MB	71	150	57
TiO$_2$ NPs	MB	97	180	58
Pani/BN nanocomposite	MB	65.7	90	59
	RhB	71.1		
h-BN/ZnO	MB	60	20	60
	RhB	82		
Non-porous BN/TiO$_2$ hybrid	RhB	67	360	61
h-BN/TiO$_2$	MB	36.3	20	62
	RhB	64		
BTF nanofibers	MB	~83.7	180	This work
	RhB	~84.3		

Fig. 5 Bacterial inhibition of BTF nanofibers at different concentrations.

antibacterial effect against both Gram positive and Gram-negative bacteria.

4. Conclusion

BTF nanofibers obtained *via* electrospinning technique were characterized in detail using FTIR, XRD, UV-vis and SEM analyses. FTIR analysis confirmed the disappearance of PVP peaks after calcination and the existence of sp^2 hybrid B–N band of BN. Additionally, XRD analysis revealed that the BTF nanofibers showed sharp patterns belonging to pure TiO$_2$ and hexagonal boron nitride phases. Furthermore, the UV-vis spectra showed that the BTF nanofibers absorbed light at 240 nm and 440 nm and exhibited a band energy of 2.81 eV. SEM images confirmed that the fibers were successfully formed and were dispersed in the form of a network after calcination. As for the performance studies, the photocatalytic activity tests showed that the BTF nanofibers offered 83.68% and 84.31% of photocatalytic degradation rate for methylene blue (MB) and rhodamine B (RhB) dyes, respectively. These results indicated that the BTF nanofibers are effective materials for the photocatalytic degradation of organic pollutants. Furthermore, antibacterial tests revealed that the BTF nanofibers were effective against Gram-

positive and Gram-negative bacteria. High concentrations of BTF nanofibers showed strong antibacterial effects against *E. coli*, *S. aureus*, *B. subtilis* and *K. pneumoniae*. Especially at a concentration of 500 μg mL^{-1}, the bacterial killing rates were quite high. As a result, the BTF nanofiber nanocomposite is considered a promising material for water treatment and bacterial control applications, exhibiting effective photocatalytic properties and strong antibacterial activity. With their superior properties, BTF nanofibers offer potential application in environmentally friendly water treatment methods and health applications.

Ethical statement

This research did not involve human or animal samples.

Data availability

Data will be made available upon request.

Conflicts of interest

The authors declare no competing interests.

References

1 H. Dhila, A. Bhapkar and S. Bhame, *Desalin. Water Treat.*, 2025, **321**, 101004.
2 S. S. Shetty, D, D, H, S, S. Sonkusare, P. B. Naik, S. Kumari N and H. Madhyastha, *Heliyon*, 2023, **9**, e19496.
3 N. Roy, T. Nivedya, P. Paira and R. Chakrabarty, *RSC Adv.*, 2025, **15**, 3008–3025.
4 J. Khodayari, K. Zare, O. Moradi, M. Kalaee and N. Mohammad Mahmoodi, *J. Photochem. Photobiol., A*, 2024, **446**, 115097.

5 F. Liang, Y.-H. Chen, H.-W. Huang, Y.-C. Chen and P.-J. Huang, *Microporous Mesoporous Mater.*, 2025, **384**, 113431.

6 S. Bikerchalen, B. Akhsassi, B. Bakiz, S. Villain, A. Taoufyq, F. Guinneton, J.-R. Gavarri and A. Benlhachemi, *J. Phys. Chem. Solids*, 2025, **196**, 112342.

7 F. Chabira, T. Mahdia, T.-I. Razika, M. Humayun, C. Ouyang, A. F. Alanazi, M. Bououdina and G. Z. Kyzas, *Polyhedron*, 2025, **265**, 117285.

8 A. Korajkic, B. McMinn and V. Harwood, *Int. J. Environ. Res. Public Health*, 2018, **15**, 2842.

9 N. Yerli-Soylu, A. Akturk, Ö. Kabak, M. Erol-Taygun, F. Karbancioglu-Guler and S. Küçükbayrak, *Eng. Sci. Technol. Int. J.*, 2022, **35**, 101175.

10 B. Sen, S. Kuzu, E. Demir, S. Akocak and F. Sen, *Int. J. Hydrogen Energy*, 2017, **42**, 23284–23291.

11 E. Erken, Y. Yıldız, B. Kilbaş and F. Şen, *J. Nanosci. Nanotechnol.*, 2016, **16**, 5944–5950.

12 Y. Yildiz, T. O. Okyay, B. Sen, B. Gezer, S. Kuzu, A. Savk, E. Demir, Z. Dasdelen, H. Sert and F. Sen, *ChemistrySelect*, 2017, **2**, 697–701.

13 K. Arikan, H. Burhan, R. Bayat and F. Sen, *Chemosphere*, 2022, **291**, 132720.

14 F. Şen and G. Gökağaç, *J. Appl. Electrochem.*, 2014, **44**, 199–207.

15 F. Gulbagça, A. Aygun, E. E. Altuner, M. Bekmezci, T. Gur, F. Sen, H. Karimi-Maleh, N. Zare, F. Karimi and Y. Vasseghian, *Chem. Eng. Res. Des.*, 2022, **180**, 254–264.

16 F. Gulbagça, S. Ozdemir, M. Gulcan and F. Sen, *Heliyon*, 2019, **5**, e02980.

17 B. Sen, B. Demirkan, A. Savk, S. K. Gülbay and F. Sen, *Int. J. Hydrogen Energy*, 2018, **43**, 17984–17992.

18 H. Burhan, K. Arikan, M. H. Alma, M. S. Nas, H. Karimi-Maleh, F. Şen, F. Karimi and Y. Vasseghian, *Int. J. Hydrogen Energy*, 2023, **48**, 6657–6665.

19 R. Bayat, E. Halvaci, T. Kozak, M. Bekmezci and F. Sen, *Fuel*, 2024, **366**, 131248.

20 G. Yavuz, E. Yilmaz, E. Halvaci, C. Catal and I. Turk, *J. Sci. Rep. C*, 2023, 1–32.

21 Ş. Çalik, A. Koç, T. Şenel, E. Zor and O. Aslan, *Uluslararası Türk Eğitim Bilim. Derg.*, 2021, **2021**, 90–113.

22 J. Jeevanandam, A. Barhoum, Y. S. Chan, A. Dufresne and M. K. Danquah, *Beilstein J. Nanotechnol.*, 2018, **9**, 1050–1074.

23 L. Otero-González, C. García-Saucedo, J. A. Field and R. Sierra-Álvarez, *Chemosphere*, 2013, **93**, 1201–1206.

24 P. Pascariu, A. Airinei, N. Olaru, L. Olaru and V. Nica, *Ceram. Int.*, 2016, **42**, 6775–6781.

25 I. Arora, H. Chawla, A. Chandra, S. Sagadevan and S. Garg, *Inorg. Chem. Commun.*, 2022, **143**, 109700.

26 J. Li and N. Wu, *Catal. Sci. Technol.*, 2015, **5**, 1360–1384.

27 F. Medjaldi, A. Bouabellou, Y. Bouachiba, A. Taabouche, K. Bouatia and H. Serrar, *Mater. Res. Express*, 2020, 7, 016439.

28 H. Chenaina, C. Messaadi, J. Jalali and H. Ezzaouia, *Inorg. Chem. Commun.*, 2021, **124**, 108401.

29 R. A. Ramos, M. H. Boratto and L. V. A. Scalvi, *Sens. Actuators, A*, 2018, **281**, 250–257.

30 I. Kitsou, P. Panagopoulos, T. Maggos and A. Tsetsekou, *Appl. Surf. Sci.*, 2019, **473**, 40–48.

31 M. Nazarkovsky, B. Czech, A. Żmudka, V. M. Bogatyrov, O. Artiushenko, V. Zaitsev, T. D. Saint-Pierre, R. C. Rocha, J. Kai, Y. Xing, W. D. G. Gonçalves, A. G. Veiga, M. L. M. Rocco, S. H. Safeer, M. V. Galaburda, V. Carozo, R. Q. Aucélio, R. J. Caraballo-Vivas, O. I. Oranska and J. Dupont, *J. Photochem. Photobiol., A*, 2021, **421**, 113532.

32 N. Thi Huyen, N. Van Tu, T. Van Hau, P. Van Trinh, C. Thi Thanh, N. Thu Loan, T. Van Tan, N. Viet Tuyen, V. Duc Chinh, V. Xuan Hoa, C. Tuan Anh and N. Van Chuc, *Mater. Lett.*, 2023, **340**, 134213.

33 A. ul Ahmad, A. Abbas, S. Ali, M. F. E-alam, Z. Farooq, Q. Abbas, M. Ahmad, A. Farid, A. Muhammad afzal, H. M. Umair Arshad, M. Javid and M. Iqbal, *Ceram. Int.*, 2021, **47**, 10089–10095.

34 M. Li, G. Huang, X. Chen, J. Yin, P. Zhang, Y. Yao, J. Shen, Y. Wu and J. Huang, *Nano Today*, 2022, **44**, 101486.

35 R. Bayat, M. Akin, M. Bekmezci, G. Gules, I. Isik and F. Sen, *Energy Technol.*, 2024, **12**(5), DOI: 10.1002/ente.202301063.

36 H. S. Karapinar, F. Kilicel, F. Ozel and A. Sarilmaz, *Int. J. Environ. Anal. Chem.*, 2021, 1–21.

37 F. Gol, A. Aygun, C. Ture, R. N. E. Tiri, Z. G. Sarıtaş, E. Kaçar, M. Arslan and F. Sen, *Bionanoscience*, 2024, **14**, 5458–5467.

38 A. Aygun, F. Gulbagca, E. E. Altuner, M. Bekmezci, T. Gur, H. Karimi-Maleh, F. Karimi, Y. Vasseghian and F. Sen, *Int. J. Hydrogen Energy*, 2023, **48**, 6666–6679.

39 F. Karimi, R. N. E. Tiri, A. Aygun, F. Gulbagca, S. Özdemir, S. Gonca, T. Gur and F. Sen, *Environ. Res.*, 2023, **218**, 114757.

40 Y. Sheng, J. Yang, F. Wang, L. Liu, H. Liu, C. Yan and Z. Guo, *Appl. Surf. Sci.*, 2019, **465**, 154–163.

41 B. Singh, G. Kaur, P. Singh, K. Singh, J. Sharma, M. Kumar, R. Bala, R. Meena, S. K. Sharma and A. Kumar, *New J. Chem.*, 2017, **41**, 11640–11646.

42 M. Nasr, R. Viter, C. Eid, R. Habchi, P. Miele and M. Bechelany, *New J. Chem.*, 2017, **41**, 81–89.

43 M. Abid, S. Sayegh, F. Tanos, H. Belaid, I. Iatsunskyi, E. Coy, M. Cretin, G. Lesage, A. Ben Haj Amara and M. Bechelany, *Colloids Surf., A*, 2023, **662**, 131043.

44 Z. Yan, J. Lin, X. Yuan, T. Song, C. Yu, Z. Liu, X. He, J. Liang, C. Tang and Y. Huang, *Sci. Rep.*, 2017, **7**, 3297.

45 S. C. Nkabinde, M. J. Moloto and K. P. Matabola, *J. Nanomater.*, 2020, **2020**, 1–10.

46 T. Balkan, Z. Guler, M. Morozova, P. Dytrych, O. Solcova and A. S. Sarac, *J. Electroceram.*, 2016, **36**, 102–111.

47 Ł. Haryński, A. Olejnik, K. Grochowska and K. Siuzdak, *Opt. Mater.*, 2022, **127**, 112205.

48 A. Aygun, R. N. E. Tiri, R. Bayat and F. Sen, *J. Hazard. Mater. Adv.*, 2024, **16**, 100464.

49 L. Lin, W. Jiang, M. Nasr, M. Bechelany, P. Miele, H. Wang and P. Xu, *Photochem. Photobiol. Sci.*, 2019, **18**, 2921–2930.

50 G. Ni, Y. Li, S. Wang and Q. Li, *Mater. Lett.*, 2021, **288**, 129385.

51 N. Wang, G. Yang, H. Wang, R. Sun and C.-P. Wong, *Front. Chem.*, 2018, **6**, DOI: 10.3389/fchem.2018.00440.

52 J.-G. Yu, J. Zou, L.-L. Liu, X.-Y. Jiang, F.-P. Jiao and X.-Q. Chen, *Desalin. Water Treat.*, 2017, **81**, 282–290.

53 S. Vadivel, M. Vanitha, A. Muthukrishnaraj and N. Balasubramanian, *J. Water Process Eng.*, 2014, **1**, 17–26.

54 Y. Fan, G. Chen, D. Li, Y. Luo, N. Lock, A. P. Jensen, A. Mamakhel, J. Mi, S. B. Iversen, Q. Meng and B. B. Iversen, *Int. J. Photoenergy*, 2012, **2012**, 1–7.

55 Y. Cui, S. M. Goldup and S. Dunn, *RSC Adv.*, 2015, **5**, 30372–30379.

56 Q. I. Rahman, M. Ahmad, S. K. Misra and M. Lohani, *Mater. Lett.*, 2013, **91**, 170–174.

57 S. Ahmad, M. S. Tahir, G. M. Kamal, X. Zhang, S. Nazir, M. B. Tahir, B. Jiang and M. Safdar, *Water*, 2023, **15**, 1788.

58 Nasikhudin, M. Diantoro, A. Kusumaatmaja and K. Triyana, *J. Phys.:Conf. Ser.*, 2018, **1011**, 012069.

59 A. Sultan, W. Raza, M. Muneer and F. Mohammad, *J. Appl. Polym. Sci.*, 2016, **133**(39), DOI: **10.1002/app.43989**.

60 X. Fu, Y. Hu, T. Zhang and S. Chen, *Appl. Surf. Sci.*, 2013, **280**, 828–835.

61 D. Liu, M. Zhang, W. Xie, L. Sun, Y. Chen and W. Lei, *Appl. Catal., B*, 2017, **207**, 72–78.

62 X. Fu, Y. Hu, Y. Yang, W. Liu and S. Chen, *J. Hazard. Mater.*, 2013, **244–245**, 102–110.

63 A. Raval, N. S. Yadav, S. Narwani, K. Somkuwar, V. Verma, H. Almubarak, S. M. Alqahtani, R. Tasleem, A. M. Luke, S. T. Kuriadom and M. I. Karobari, *J. Funct. Biomater.*, 2023, **14**, 201.

64 A. Kilic, L. Beyazsakal, B. T. Findik and H. Incebay, *Inorg. Chim. Acta*, 2020, **510**, 119777.

65 P. Aruna, P. Lalitha and K. Muddukrishnaiah, *Microb. Pathog.*, 2025, **199**, 107197.